www.sciencemag.org/content/346/6210/739/suppl/DC1

Supplementary Materials for

Neoarchean carbonate-associated sulfate records positive $\Delta^{33}S$ anomalies

G. Paris,* J. F. Adkins, A. L. Sessions, S. M. Webb, W. W. Fischer

*Corresponding author. E-mail: gparis@caltech.edu

Published 7 November 2014, *Science* **346**, 739 (2014)
DOI: 10.1126/science.1258211

This PDF file includes:

Other Supporting Online Material for this manuscript includes the following:
(available at www.sciencemag.org/content/346/6210/739/suppl/DC1)

Material and methods:

Geological context

The Neoarchean Campbellrand platform from the Transvaal Supergroup in South Africa is one of the oldest, best-studied carbonate platforms in the Archean sedimentary record (*32*). The Neoarchean to early Paleoproterozoic Transvaal Supergroup is preserved in two distinct structural basins (Griqualand West and Transvaal) over an area of 0.2×10^6 km^2 (Fig. S1). In Griqualand West, the Transvaal Supergroup is divided into three distinct subgroups—the middle of these, the Campbellrand Subgroup, is represented by an extensive, ~2 km thick marine platform. The platform began as a carbonate ramp and developed into a mature rimmed carbonate shelf that spread across the entire Kaapvaal Craton through the stacking of numerous progradational cycles (*36*). Eventually the carbonate platform drowned during a major transgression, reflected in the deposition of iron formation units of the Asbestos Hills Subgroup across the craton.

Compared to most rocks of this age, the Campbellrand platform is strikingly well preserved. It remains flat-lying across much of the ancient craton, particularly in Griqualand West, where metamorphism was limited to sub-greenschist facies equivalent (*36*). Though the behavior of sulfur isotopes in CAS during true high temperature metamorphism is not known, such a metamorphic path is not unusual in CAS studies from younger successions [e.g. (*37*)]. Steep structural dips (and higher metamorphic temperatures) occur around the Bushveld Igneous Complex, and acute folding and faulting appear along the western edge of the craton, where Proterozoic red beds of the Olifantshoek Group are thrust over Campbellrand rocks (*32*). Petrographic textures in carbonate lithologies are commonly preserved by fabric-retentive, early diagenetic dolomite, though in many areas, calcite remains (*31, 32, 38*).

A detailed sequence stratigraphic framework for the Campbellrand-Kuruman sedimentary succession has been previously assembled, built on inferences from the unique carbonate sedimentology consisting of a substantial amount *in situ*, benthic carbonate precipitation (*31, 32, 38-44*). This style of carbonate sedimentation is useful because these marine cements offer an attractive archive of the isotopic composition of seawater sulfate across the platform (*45*). Carbon and oxygen stable isotope data from carbonates sampled at high-resolution from different paleoenvironments on the platform provide context for understanding carbonate diagenesis (*31*).

Key aspects of the sedimentary geology as it relates directly to the sections in this study are summarized as follows. The platform can be broadly divided into two large sequences, the Lower Nauga/Reivilo and the Upper Nauga formations, each representing aggradational packages separated by a thin transgressive unit comprised in part of a thin iron formation-rich sequence at the top of the Lower Nauga/Reivilo Formation. Carbonate deposition was reestablished by the time of the Upper Nauga Formation. During Upper Nauga time, the Campbellrand platform slope was at its steepest, with a lagoon that developed episodically behind the reef margin. Immediately above these facies, a major transgression led to the ultimate demise of the Campbellrand platform, as carbonate deposition was slowly outpaced by accommodation. This transgression is recorded within the Gamohaan Formation, in a sequence characterized by deep subtidal fenestral microbialites with increasing chert content that ultimately grade into iron formation of the Kuruman Formation, which was subsequently deposited across the entire Kaapvaal Craton.

Our CAS data comes from samples collected from three different stratigraphic sections. Section W1 captures shallow subtidal paleoenvironments of the Reivilo Formation at Boetsap (*38, 46, 47*), during the early development of the Campbellrand platform. Textures consist of minor grainstones and abundant precipitated stromatolites including seafloor aragonite fans. Most of the carbonates in this part of the platform have been altered with a fabric-retentive dolomitization, though in this section some horizons still remain limestone—a comparison of dolomite and calcite CAS values closely agree (Table S3). Section W2 is located at Kuruman Kop (*38, 46*) and captures the terminal drowning of the carbonate platform with a subtidal microbialite facies that includes abundant early marine cements (Fig. S1). The deep subtidal, fenestral microbialite facies of the 2.521 Ga Gamohaan Formation contains abundant herringbone calcite (*22, 43, 48*). Herringbone calcite comprises a texture of early marine cements composed of staggered alternating bands of light and dark elongated length-slow calcite (probably originally as Mg-calcite, now as low Mg-calcite or dolomite) crystals (*42*); and in the Campbellrand platform it occurs as encrusting beds and an important phase of void-filling cementation associated with the deep subtidal fenestral microbialites (*22*). These early marine cements provide an attractive and important fabric for recording seawater sulfate in subtidal environments on the Campbellrand platform. The third section GKP01 comes from a drill core through proximal slope facies of the Campbellrand platform collected with the Agouron Institute South African Drilling Project (*39*). Here we also targeted herringbone calcite in the Upper Nauga Formation where those cements developed associated with deep subtidal fenestral microbialites.

Sample preparation and petrographic observations

Samples were cut with a rock saw orthogonal to bedding, and the resulting two bookmatched slabs were marked to preserve orientation. Powder samples for isotopic analysis were collected by micromilling from one slab, and corresponding ~25 μm-thick sections for petrography were collected from the same area of the matching slab. Slabs were cleaned with MilliQ water then drilled using a Sherline 5410 mill equipped with a RoundTool diamond-coated carbide end mill (GR4SI 1/16 D1; 1.5mm diameter) to collect 40 to 150 mg of powders from different petrographic textures. Microscopy was performed using natural, cross-polarized and reflected light to assess the relative abundance of pyrite and kerogen within different sample textures. Four of these samples were additionally screened by scanning electron microscopy (SEM), which offers finer resolution and a more sensitive detection of pyrite (Fig. S4).

SEM observations were performed using the ZEISS 1550VP field SEM operated with a working distance of 8 mm and an electron high voltage of 15 kV. Backscatter photomicrographs were taken with a quadrant backscatter detector (QBSD). Secondary electron photomicrographs were taken with a SE2 detector. Elemental analyses and composition maps were obtained with an Oxford X-Max 80mm^2 energy-dispersive X-ray silicon drift detector (SDD EDS). Compositional maps were used to discriminate calcite from dolomite. Many samples from W1 show textures preserved in fabric-retentive dolomite and rarer calcite. Samples from W2 largely remain calcite with abundant herringbone cements. Pyrite is visually absent from the herringbone calcite textures.

X-ray Absorption Spectroscopy

X-ray absorption spectroscopy (XAS) is a powerful technique used to observe the chemical environments of specific elements within a sample. We applied this approach to directly observe the redox state of S present in our Late Archean carbonate samples and assess whether these rocks indeed contain measurable amounts of CAS. To prevent oxidation

of any reduced S present in the samples, we used an anaerobic glove box and vacuum bags to prepare the samples. A micro-rotary drill with a 1 mm drill bit was used to produce powders of sample textures, producing ~20-100 mg of powder. The samples were loaded into small glass vials then transferred to an anaerobic chamber wherein they were deoxygenated, returned to the anaerobic glass vials, and then stored in heat-sealed Mylar bags for transit to the beam line. In addition, several samples (W2_80m_b, GKP_a, GKP_b) were prepared at the beam line using a micro-rotary drill and immediately analyzed to test for oxidation during sample preparation (no significant differences were observed). Several mg of powder were placed onto sulfur-free (< 1 ppm) tape in a milled aluminum sample holder, and placed in He atmosphere for analysis. X-ray absorption near edge structure (XANES) spectra for bulk S valence state were collected at beamline 4-3 at Stanford Synchrotron Radiation Lightsource (SSRL) in Menlo Park, California. A silicon 111 $\Phi = 90$ crystal was used and X-ray absorption spectra (XAS) was collected on a Vortex fluorescence detector. A collimating mirror was used to help reduce harmonics in the beam, and a sodium thiosulfate (NaS_2O_3) standard was used for energy calibration. Multiple repeats through the S K-edge were run on all samples by measuring fluorescence while scanning from 2.43 to 2.70 keV, and averaged to obtain better spectral resolution. Multiple repeats show no evidence of any photooxidation or redox changes during analysis.

We fit the sample spectra for the energy range 2.45 to 2.53 keV using standards to estimate the relative abundance of different S phases (sulfate, pyrite, and organic sulfur) in the samples (Fig. S5). The carbonate-associated sulfate (CAS) standard is a deep-sea coral, which provides a commonly used external isotopic standard in the Adkins lab. Pyrite and dibenzothiophene (a proxy for organic sulfur in Archean kerogen) standard spectra were taken from the European Synchrotron Radiation Facility (ESRF) S XANES database, http://www.esrf.eu/UsersAndScience/Experiments/Imaging/ID21/php) (*49*). Estimates of the relative abundances of S-bearing phases can be found in Table S4. Importantly, even though the XANES data consistently revealed the presence of other reduced S-bearing phases, sulfate was detectable in all Archean carbonate samples analyzed. This confirms that CAS is a native phase in low abundance in these rocks, and illustrates both the existence of a viable proxy archive as well as the importance of small-sample sizes and texture-specific measurements.

Carbon and oxygen isotope analysis

The carbon- and oxygen-isotopic compositions of carbonates were measured at Caltech on a Thermo Scientific Delta-V isotope ratio mass spectrometer equipped with a Gasbench II introduction system. Results are presented using δ-notation, expressed as permil (‰) deviations in the $^{13}C/^{12}C$ or $^{18}O/^{16}O$ ratios of a sample with respect to the Pee-Dee Belemnite (VPDB) standard. The Carrera Marble standard reproduced to ±0.11‰ (2SD, n=8) for $\delta^{13}C$ values and ±0.19‰ (2SD, n=8) for $\delta^{18}O$ values.

CAS isolation

All plastics (centrifuge tubes, autosampler vials and Biorad columns) were leached in 10% reagent grade HCl and rinsed 5 times in MilliQ water. Savillex vials were cleaned in 5% Seastar HNO_3, rinsed 5 times in MilliQ water, refluxed overnight with concentrated Seastar HNO_3 at 160°C and rinsed 3 times in MilliQ water. For each sample, 40 mg of powder were weighed and sonicated for 60 min in 0.6 M NaCl, with the exception of samples 2 to 11 that were first soaked in a solution of 30% H_2O_2 and 1M NaOH for 30 min and rinsed 3 times in MilliQ water. All samples were then centrifuged and rinsed 4 times in MilliQ

water. After drying, the samples were weighed again, dissolved in 30% v/v HCl, centrifuged, and the supernatant was collected in a Savillex Teflon vial. The supernatant was dried at 120°C on a hot plate under laminar flow and the insoluble residue was dried in an oven at 90°C. Both residues were weighed, and the dried supernatant was dissolved in HCl. Biorad disposable columns were loaded with 2 ml of clean AG1X8 anion-exchange resin. Once in the column, the resin was cleaned with 20 ml of 10% v/v HNO_3, 20 ml of 30% v/v HCl and 20 ml of 1.5% v/v HCl. Samples were loaded, cations were removed by rinsing the column with 3 times 5 ml of MilliQ water, and sulfate was eluted with 3×4 ml of 0.5 M HNO_3.

The sulfate extraction protocol was adapted from Das et al. (*50*). We did a series of elution tests on anion exchange columns using a solution of 6.5 grams of aragonitic deep-sea coral, from an individual similar to the one analyzed in (*20*), dissolved in 10% HCl. The first test ran the equivalent of 23 mg of dissolved aragonite through the column to ensure complete release of sulfate from the column after two water rinses (Fig. S6A). A second test used 30 mg of coral equivalent through 1.5 ml of resin, with a third MilliQ wash of the resin (Fig. S6B), demonstrating that no sulfate was released before elution.

Seawater and corals were run through the columns following the same procedures. The advantage of using anion exchange resin AG1X8 over cation resin AG50X8, as described in (*15*), was a significantly lower blank. With this new protocol, the blank is globally lower but with some variability, so its concentration was measured for each batch of columns (Table S1). Blanks and concentrations of sulfate were measured using a Dionex ICS 2000 ion chromatography system.

Sulfur isotope ratio measurements

Sulfur isotopes were measured as $^{32}S^+$, $^{33}S^+$ and $^{34}S^+$ ions on a Thermo Neptune Plus multi-collector inductively-coupled plasma mass spectrometer (MC-ICPMS) in high resolution mode equipped with a desolvating membrane (Aridus, Cetac) to decrease interferences, following the method described in (*20*). Samples were calibrated by sample-standard bracketing to correct instrumental fractionation. The bracketing standard was a 20 µmol/l Na_2SO_4 solution. Na^+ was added to the samples after purification as NaOH to match the sodium concentration of the bracketing standard. The sulfur-isotope ratio of the Na_2SO_4 bracketing solution was determined by comparing it directly to a solution of international standard IAEA-S1 ($\delta^{34}S_{VCDT}$ = -0.3‰, $\delta^{33}S_{VCDT}$ = -0.055‰, (*51, 52*). The $\delta^{34}S_{VCDT}$ value of our bracketing Na_2SO_4 solution is -1.55‰±0.16 (2sd) and the $\delta^{33}S_{VCDT}$ value is -0.77±0.17‰ ($\Delta^{33}S$ = 0.02±0.17‰). All values were corrected assuming linear drift and corrected for instrumental background.

Consistency standards (seawater and a deep-sea coral aragonite, (*20*) , Table S2) were purified and measured alongside the Archean carbonates. Most of the samples textures were too small to allow replicates of the same micromilled powder. Triplicates in Table S3 are based on 40mg aliquots of a bigger batch of powder from the same texture. Sample 11 was replicated after redissolution of a larger amount of powder. The overall external reproducibility for sample 11 demonstrates the typical external reproducibility for $\delta^{34}S$ and $\Delta^{33}S$ values (2σ is 0.22‰ and 0.51‰ respectively for samples before blank correction.

Blank correction and assessment of analytical uncertainty

Uncertainties for sulfur isotopic compositions are given as blank-corrected 2 standard deviations. Blanks come in two forms, a machine blank from the MC-ICPMS that is

subtracted using bracketing blanks, and a total procedural blank (TPB) that includes reagents and sample handling. To measure the TPB we processed empty vials through the whole procedure. Typically there is not enough sulfur to run both the IC and the ICPMS for TPB samples. We usually run them through the IC to monitor the size of our blank (Table S2), but in two cases we ran them on the MC-ICPMS instead, and report the results here ($\delta^{34}S$=11.73±3.61‰, $\delta^{33}S$=5.98±1.95‰ and $\Delta^{33}S$=-0.05±0.10‰). We used these numbers in the following TBP correction equations as ratios ($^{34}R_{blk}$) and not delta values to correct the isotopic ratio ($^{34}R_{meas}$) to the true CAS isotopic ratio ($^{34}R_{carb}$):

$$^{34}R_{meas} \times n_{meas} = {}^{34}R_{blk} \times n_{blk} + {}^{34}R_{carb} \times n_{carb} \quad (1),$$

where n_{meas} is the total mass of sulfur from a single sample and

$$n_{carb} = n_{meas} - n_{blk} \quad (2).$$

The true isotopic composition of our sample, $^{34}R^{i}_{carb}$, and concentration of our sample, ppm^{i}_{carb}, were calculated as:

$$^{34}R_{carb} = (^{34}R_{meas} \times n_{meas} - {}^{34}R_{blk} \times n_{blk})/n_{carb} \quad (3)$$

and

$$[SO_4^{2-}]_{carb} = (n_{carb} \times 96.04) / m_{carb} \quad (4),$$

with m_{carb} the mass of carbonate collected for each experiment.

Uncertainty in the TPB corrected ratio was calculated by propagating the standard deviation obtained for random populations of 1000 values with a normal distribution characterized by the standard deviation estimated for each member of equation (3) and (4). An analogous set of equations can be written for $R^{33}S_{carb}$. The blank correction increases the typical $\delta^{34}S$ reproducibility from 0.22 to 0.35‰ and the $\Delta^{33}S$ one from 0.51 to 0.70‰.

Cleaning of the sample prior to analysis

We know from microscopy (light and electron) and XANES analyses that our rocks contains sulfate, but also other S-bearing compounds. We therefore tried to understand how to best prepare our samples before sulfate extraction and to evaluate the influence of chemical cleaning on our samples. We drilled the microbial laminae of sample W2_80 and split the powder into multiple aliquots for parallel treatments. Such tests require a bigger mass of sample than usually drilled for our analyses (~250 mg), which makes it difficult to ensure that the powder is homogeneous. Half of the splits were leached in 1 ml of 0.6 M NaCl for one hour in an ultrasonication bath, rinsed three times with MilliQ water, reacted in 1ml of 50/50 mixture of 30% H_2O_2 and 1M NaOH for 30 min at room temperature, and rinsed again four times in MilliQ water, the other half were left uncleaned. All splits were then dissolved in 5% HCl. Except for one cleaned and one uncleaned split, all samples were centrifuged and the supernatant was separated from solid residuals. All samples, including the uncentrifuged splits, were analyzed for sulfur isotopic composition and CAS concentration (Fig. S7 A, B). Within measurement uncertainty, the chemical cleaning technique does not affect the results. The main difference seems to arise from the choice of centrifuging or not. Uncentrifuged samples exhibit higher concentrations as well as higher $\Delta^{33}S$ values. Values for $\delta^{34}S$ vary between 12 and 14 ‰ and do not correlate with 1/[CAS], whereas $\Delta^{33}S$ values are correlated with 1/[CAS], suggesting the addition of a S phase bearing similar $\delta^{34}S$ values but a more positive MIF signal in the solid residuals. Either the residues contained reduced sulfur that was oxidized during loading on the column or the observed variability reflects heterogeneity within the sample. The latter is supported by a comparison to samples from the same stratigraphic layer that went through a simple NaCl leach.

In order to avoid artifacts due to possible oxidation of trace amounts of pyrite or organic sulfur, we therefore chose to use only a NaCl leach for most of the samples (note however that samples 2 to 11 have been oxidatively cleaned before the NaCl leach, with no difference apparent in the results). Additionally, the K-edge profiles show that our samples contain sulfate, organic sulfur, and pyrite. Because our samples are extremely small, they are dissolved in a few ml of 1.5 M HCl. The dissolving rock degasses CO_2 instantaneously. If pyrite gets dissolved, H_2S would too degas quickly, with no time to oxidize and remain in the solution. If pyrite does not dissolve, it would be removed during centrifugation. If the difference between treatments in the cleaning text is caused by mixing between the different S phases present in the sample, this would suggest indeed that the reduced S phase in our samples gets oxidized and measured with sulfate only when the residues are loaded onto the column.

To provide additional context for these results, we plotted them with samples from the main data set that fall at the same stratigraphic interval as the hand sample used for the cleaning test. One microbial laminae texture, drilled from the same hand sample as the cleaning tests (diamond in Fig. S7 C, D) and taken through a full cleaning procedure, shows higher sulfate concentration and slightly elevated $\Delta^{33}S$. Two textures from a separate hand sample, with only NaCl cleaning, show even more elevated $\Delta^{33}S$ and higher CAS concentration despite centrifugation. Importantly, these data show just as much heterogeneity in our powders at small scales as between different cleaning approaches.

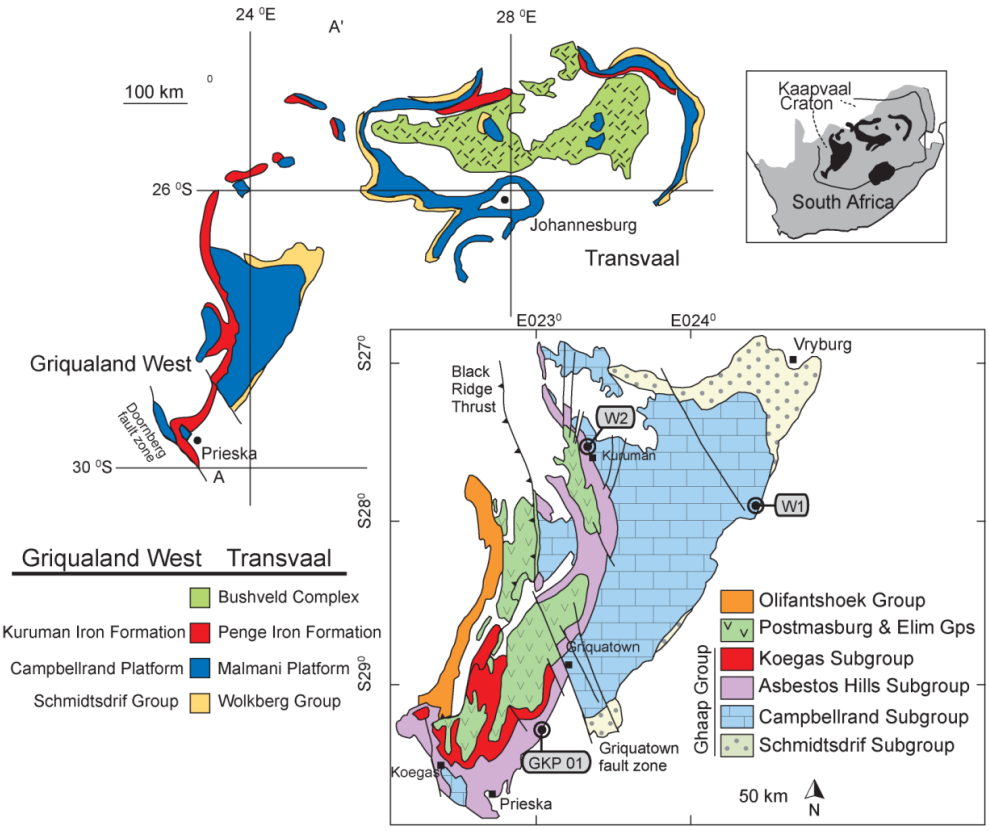

Fig. S1.

Geologic map of Kaapvaal Craton (modified from (*53*)) showing the surface exposures of the Late Archean Transvaal Supergroup, broadly divided into two structural sub-basins. The inset contains a detailed close-up map of the stratigraphic sections in Griqualand West where the samples were collected.

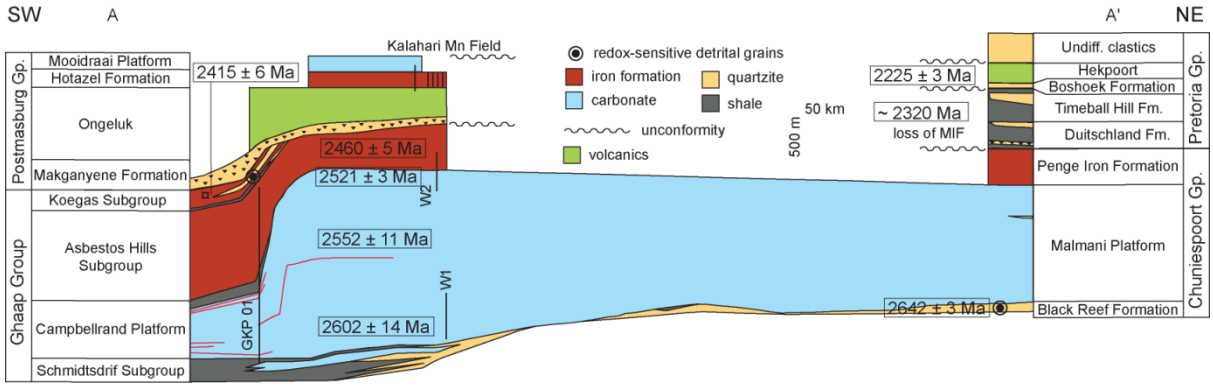

Fig. S2.

Cross-section through the Campbellrand platform from A to A' (Fig. S1), showing the generalized stratigraphy of the Transvaal Supergroup with key geochronological constraints and the stratigraphic and paleoenvironmental breadth of sections W1, W2, and GKP01 shown (modified from (*54*)).

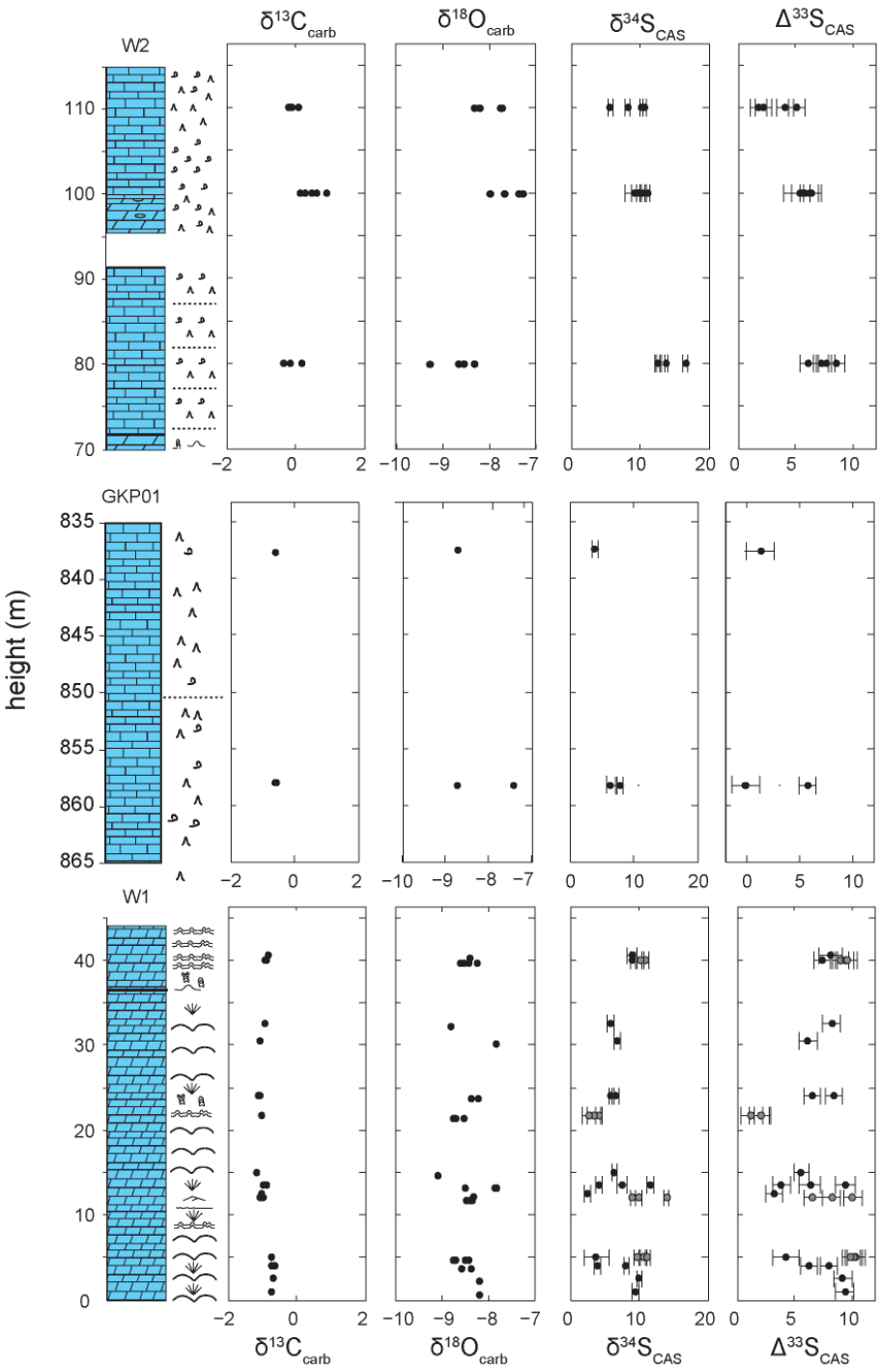

Fig. S3.

Lithostratigraphy of W1, GKP01, and W2 ordinated according to their relative age (from bottom to top) with geochemical data plotted alongside. Grey-filled circles mark triplicate analyses of the same powder and show in some cases variability beyond analytical uncertainty (at 12 m), suggesting small-scale variability of the isotopic composition of CAS in some samples. Error bars plotted as 2SD.

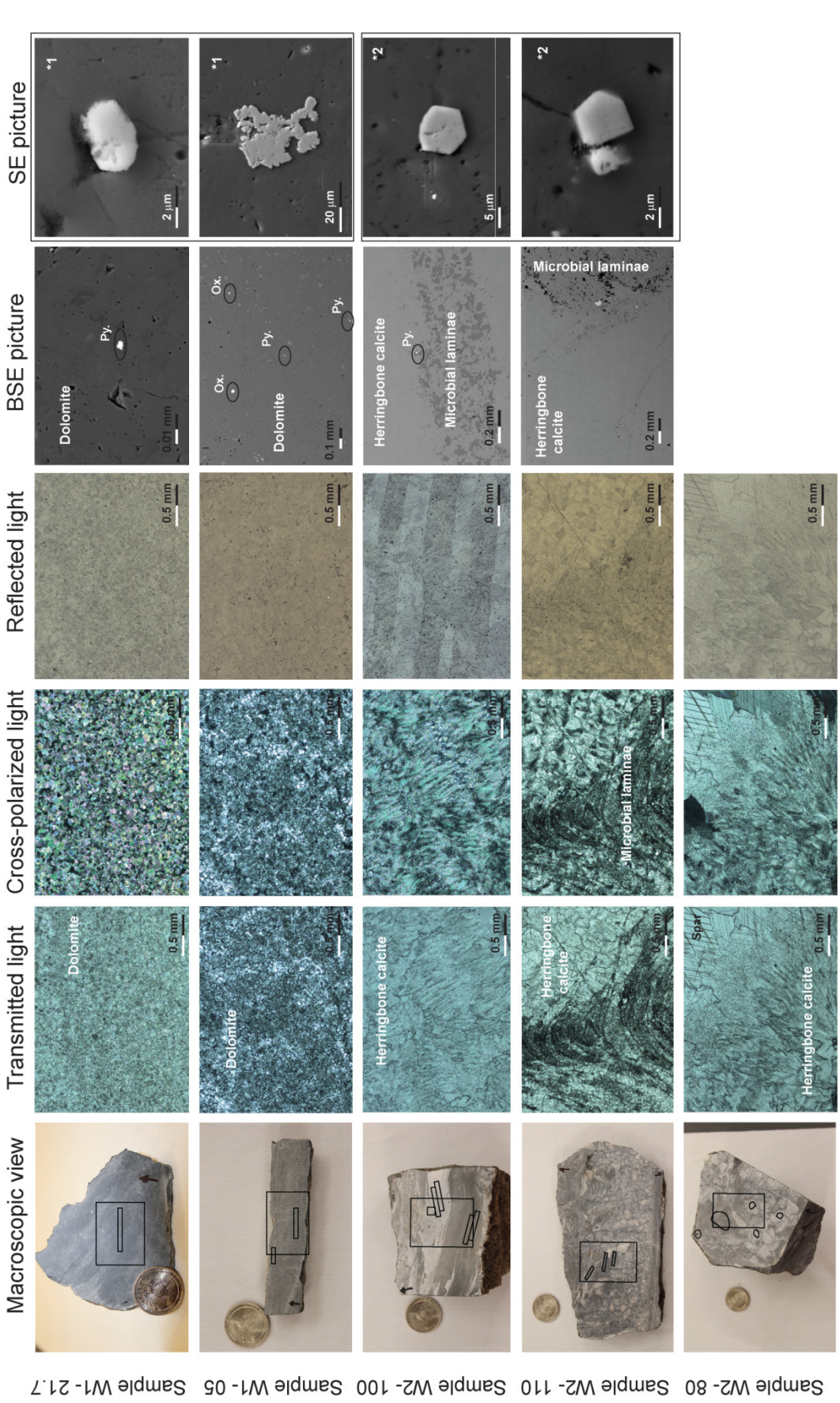

Fig. S4.

Petrographic images of sample textures collected from stratigraphic sections. From top to

bottom, samples W1-21.7, W1-80, W2-100. W2-110 and W2-80. Sample W1-21.7: shallow subtidal precipitated stromatolites and aragonite crystal fans, now dolomite. Sample W1-05: shallow subtidal precipitated stromatolites with occasional grainstone laminations. Sample W2-100, 110, 80: deep subtidal fenestral microbialites with abundant herringbone calcite marine cements growing from microbial laminae and light-colored late void-filing sparry cements. From left to right: cut and polished slabs with black boxes denoting locations from which different textures were microsampled (coin for scale), transmitted light images of thin sections cut directly from the opposing face of the sample (scale 50X), transmitted cross-polarized light images of the same textures, reflected light images of the same textures (note the lack of pyrite grains), backscatter electron (BSE) images of sample textures show rare grains with high backscatter composed primarily of oxides, apatite and (more rare) pyrite and close-up secondary electrons (SE) views of pyrite grains. Only two samples were investigated with SE, W1-21.7 (*1) and W2-100 (*2).

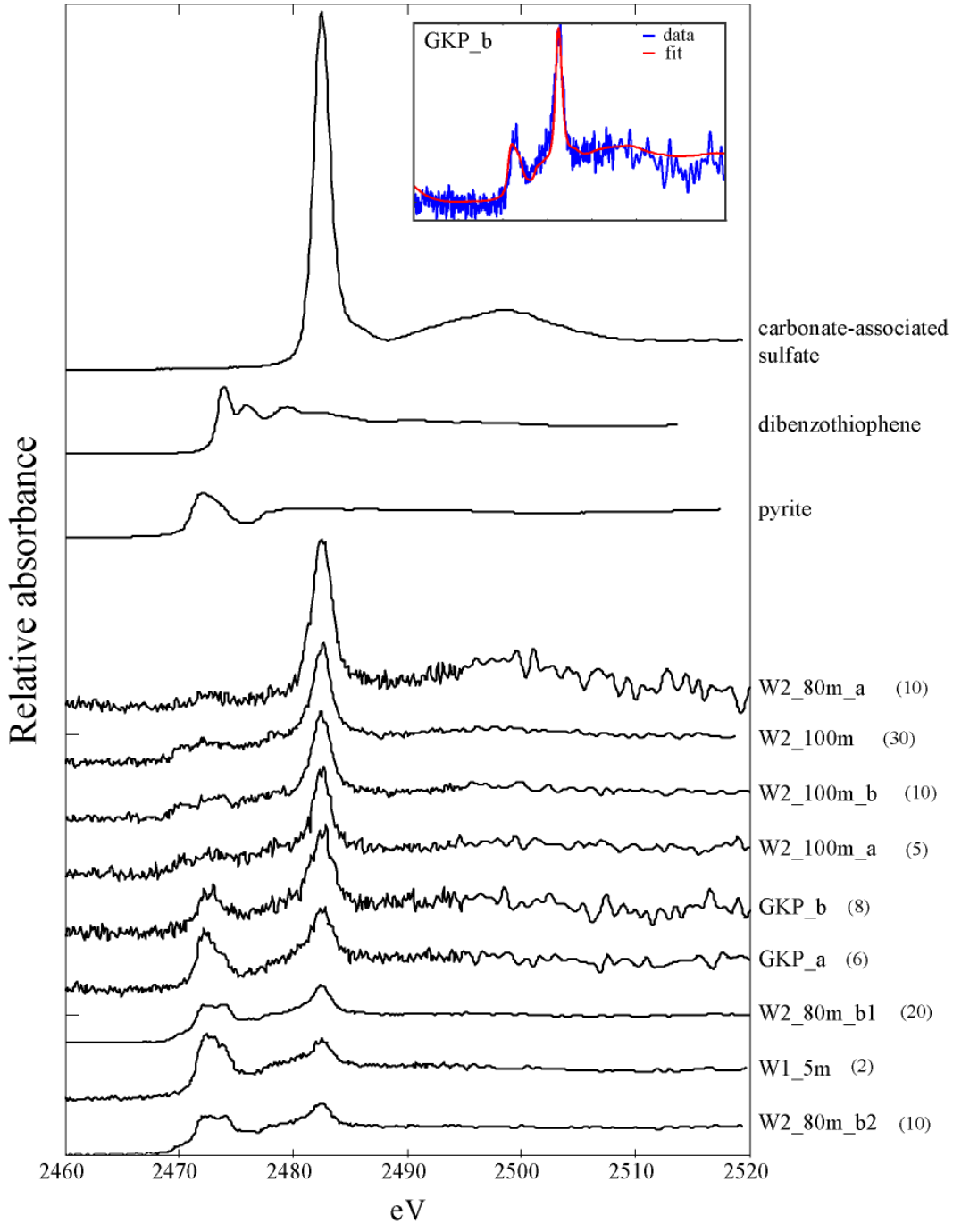

Fig. S5.

XANES spectra of carbonate samples from this study. Sample names are listed on the right. Number of repeats through the K-edge are shown in parentheses next to the sample names. CAS, pyrite, and organic sulfur (dibenzothiophene) standards are shown on top. An example of spectra-fitting is shown inset for drill core sample GKP_b.

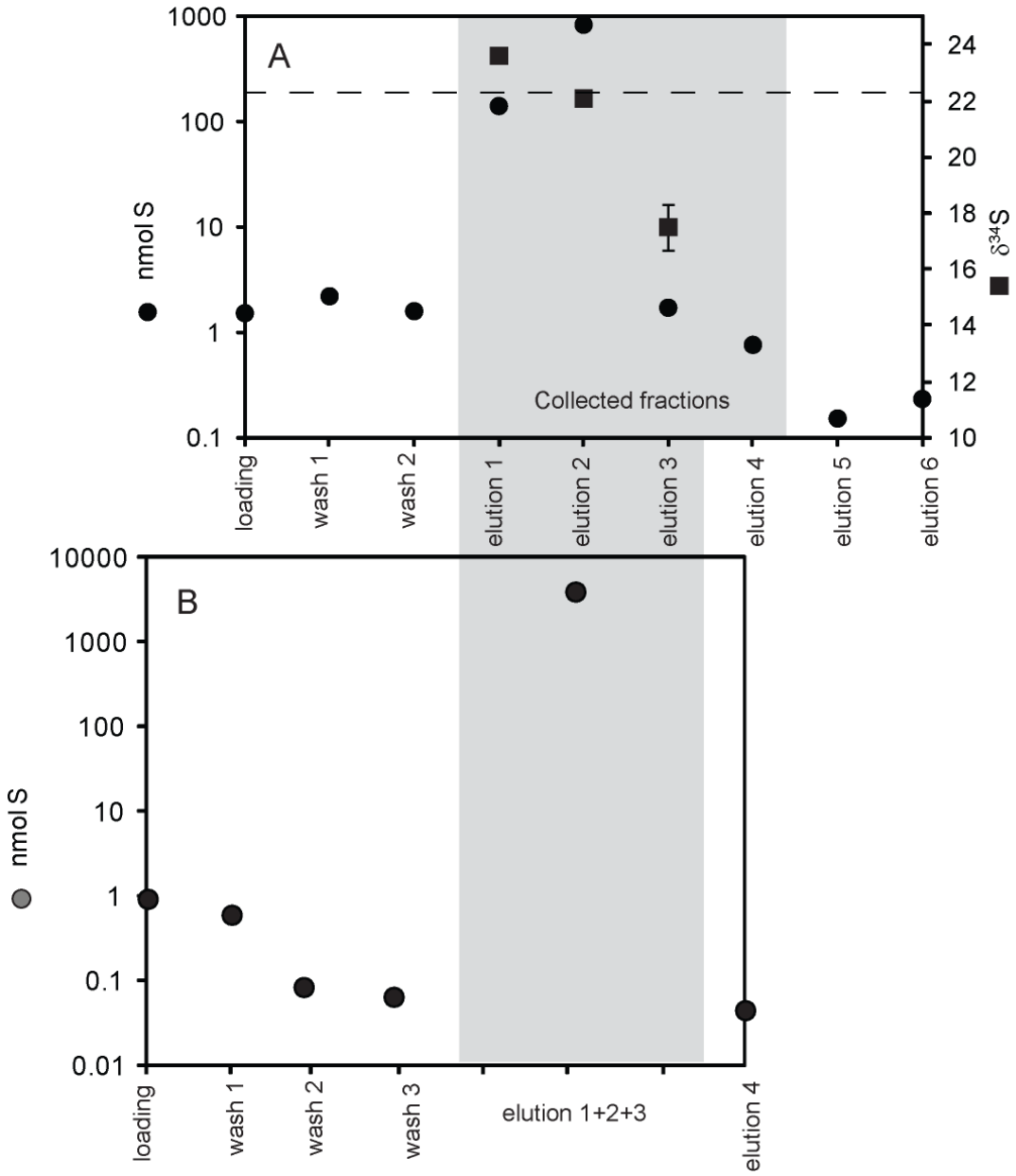

Fig. S6.

Sulfate elution curves for our anion exchange resin. Collected fractions using 1.5 ml of AG1X8 strong anionic resin, introducing 23 mg (A) and 30 mg (B) of dissolved carbonate. Each wash consisted of 2 CV (column volumes, here 1.5 ml) of MilliQ water and each elution of 2 CV of 0.5 M HNO_3. Figure S6A shows that three elutions of 0.5 M HNO_3 remove all sulfate from the resin. Each elution is slightly fractionated but the total collection is not (dashed line). Figure S6B shows that even with a larger amount of carbonate loaded, and a third wash of MQ, sulfate is retained. Error bars are 2SD.

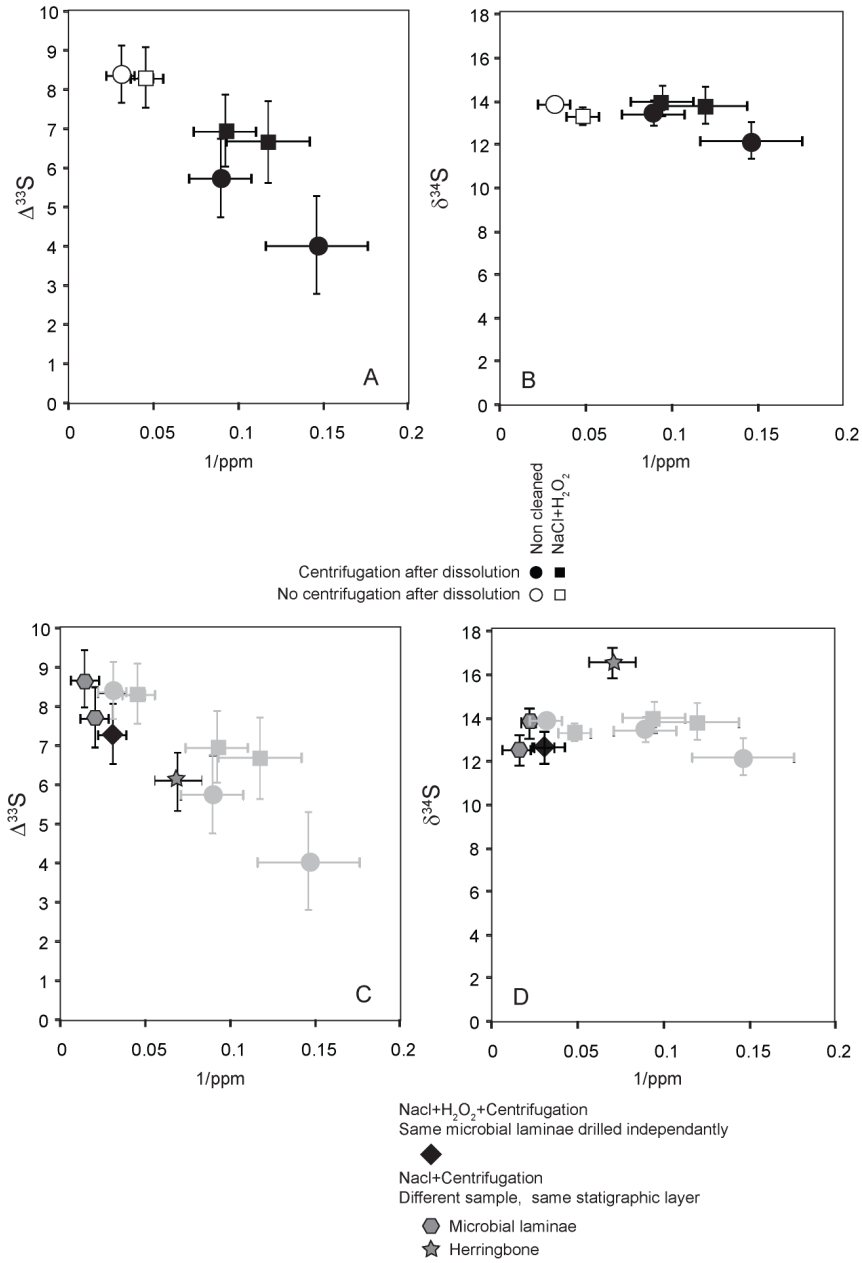

Fig. S7.

(A, B) Cleaning test results for sample W2-080. All of the tests come from powder drilled from the same microbial laminae and went through either full cleaning (squares) or no cleaning at all (circles), followed by centrifugation (open symbols) or not (closed symbols). (C, D) Comparison of the cleaning test results with data from the same stratigraphic interval. One sample is from the same microbial laminae texture as the cleaning powder (diamond), and it was fully cleaned. The other three are from a separate hand sample and only rinsed in NaCl.

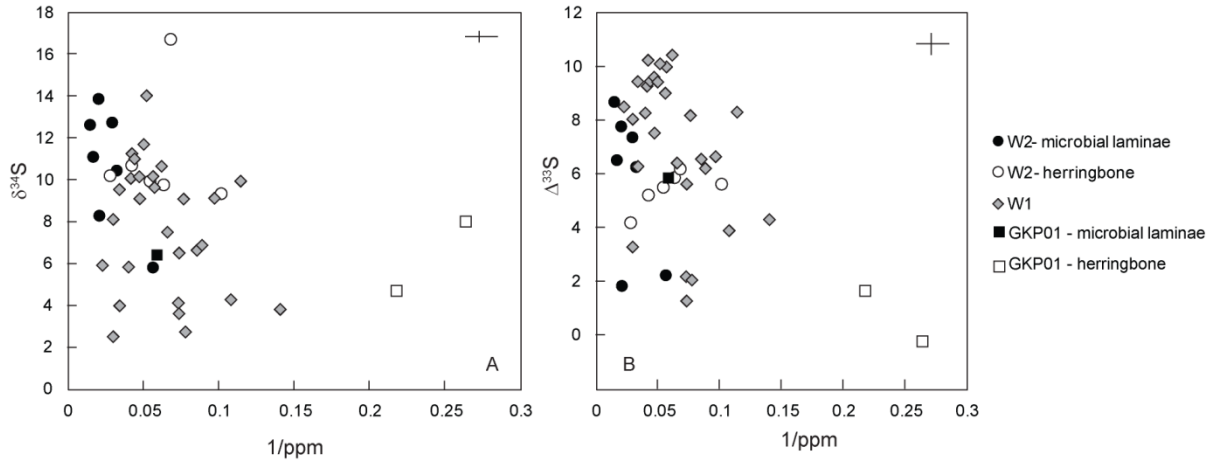

Fig. S8.

A- crossplot of $\delta^{34}S$ vs. 1/[SO4], B- crossplot of $\Delta^{33}S$ vs. 1/[SO4]. Data are broken out by lithology and texture: dolomite W1 (diamonds), microbial mats (closed symbols) or herring bone (open symbols) for W2 (circles) and the drill core samples (squares). Average error bars are given in the corner of each plot (10% on concentrations, 0.35‰ for $\delta^{34}S$ and 0.70‰ for $\Delta^{33}S$).

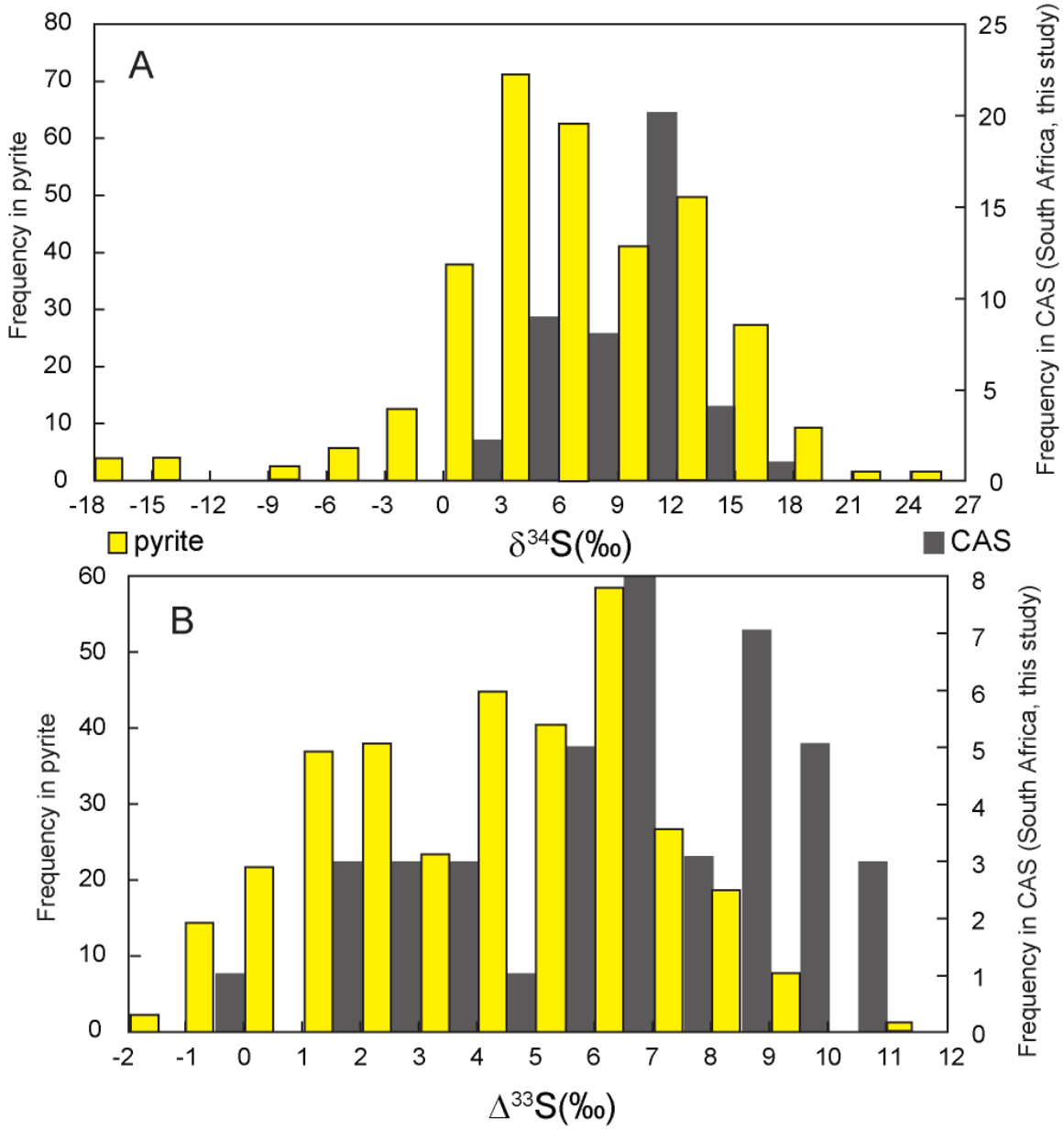

Fig. S9.

Histograms comparing the distribution for $\delta^{34}S$ (A) and $\Delta^{33}S$ (B) between CAS measured in this study (grey bars) and disseminated pyrite measured in the Campbellrand formation (yellow bars) (*4, 23-30*). The histograms show a different distribution of the CAS data, which is shifted towards more positive values for both $\delta^{34}S$ and $\Delta^{33}S$. Our CAS data exhibit mean $\delta^{34}S$ and $\Delta^{33}S$ values of 8.59 ± 3.24‰ (n=44) and 6.39 ± 2.79‰ (n=44), respectively, whereas disseminated pyrite data give mean values of 4.48±7.15 (n=346) and 4.48±2.60 (n=336).

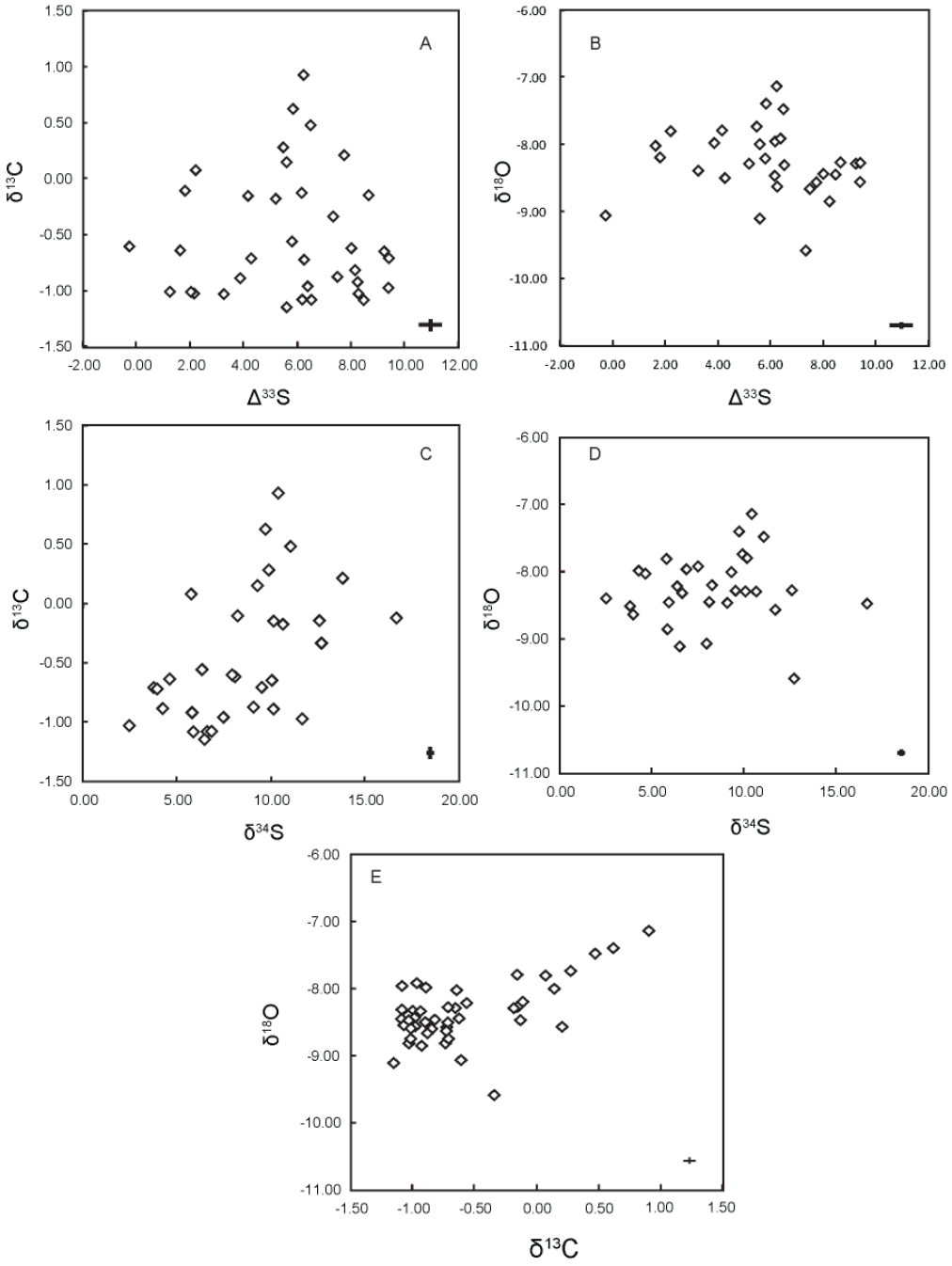

Fig. S10.

Relationships between carbon and oxygen isotopes and sulfur isotopes [$\Delta^{33}S$ vs. $\delta^{13}C$ (A) and $\delta^{18}O$ (B), $\delta^{34}S$ vs. $\delta^{13}C$ (C) and $\delta^{18}O$ (D) and $\delta^{13}C$ vs. $\delta^{18}O$ (E)]. Comparison of limestone and dolomite (fabric-retentive) samples from the same stratigraphic horizon reveals very similar isotope data and suggests preservation of CAS through early dolomitization. Typical 2SD error bars are given in the corner of each plot. C and O units in permil VPDB, S units in permil VCDT.

	nmol	sd (n=3)
Batch 1	0.60	0.45
Batch 2	0.37	0.02 (n=4)
Batch 3	0.54	0.20
Batch 4	0.16	0.02
Batch 5	0.23	0.06

Table S1.

Blank variability, measured by Ion Chromatography. Each batch corresponds to a group of samples. For each batch, the amount of sulfate (nmol) is provided together with the standard deviation of the population of blanks analyzed.

	$\delta^{34}S$	2sd	$\Delta^{33}S$	2sd	
Coral batch 1	22.25	0.23	0.12	0.01	n=2
Coral batch 2a	22.21	0.12	-0.05	0.07	n=2
Coral batch 2b	22.23	0.07	0.02	0.13	n=3
Coral batch 3	22.19	0.26	0.05	0.32	n=9
Coral batch 4	22.18	0.11	0.09	0.16	n=5
Coral batch 5	22.24	0.14	-0.05	0.15	n=5
SW 1	21.00	0.17	0.02	0.09	n=4
SW 2	20.98	0.13	0.11	0.11	n=6
Sample 11-a	12.75	0.10	0.55	7.17	n=2
Sample 11-b	12.65	0.26	0.52	6.97	n=3

Table S2.

Isotopic compositions for coral and seawater consistency standards and Archean sample replicates.

sample	texture	drilling location	%sulfate	%pyrite	%organic
W2_80m_b2	deep subtidal microbial laminae	Caltech	7	78	15
W1_5m	seafloor aragonite crystal fan, now dolomite	Caltech	9	75	16
W2_80m_b1	deep subtidal microbial laminae	SLAC	9	76	15
GKP_a	microbialite herringbone calcite	SLAC	15	80	5
GKP_b	draping calcite	SLAC	22	75	3
W2_100m_a	deep subtidal microbialite herringbone calcite	Caltech	27	60	13
W2_100m_b	deep subtidal microbialite herringbone calcite	Caltech	26	50	24
W2_100m	deep subtidal microbial laminae	Caltech	30	60	10
W2_80m_a	deep subtidal microbialite draping calcite	Caltech	50	45	5

Table S3.

Abundances of S-species in selected samples as determined by fitting the S K-edge X-ray absorption spectra shown in Fig. S5.

Additional Data table S1 (separate file)

Summary of $\delta^{13}C$, $\delta^{18}O$, $\delta^{34}S$ and $\Delta^{33}S$ values. Error for $\delta^{13}C$, $\delta^{18}O$ is 0.1 ‰ (2sd) and relative standard deviation for concentration is 10%. *Samples in italic are replicates aliquoted from the same powder and illustrate possibilities of small scale variability.

References and Notes

1. J. Farquhar, H. Bao, M. Thiemens, Atmospheric influence of Earth's earliest sulfur cycle. *Science* **289**, 756–758 (2000). Medline doi:10.1126/science.289.5480.756

2. Y. Ueno, M. S. Johnson, S. O. Danielache, C. Eskebjerg, A. Pandey, N. Yoshida, Geological sulfur isotopes indicate elevated OCS in the Archean atmosphere, solving faint young sun paradox. *Proc. Natl. Acad. Sci. U.S.A.* **106**, 14784–14789 (2009). Medline doi:10.1073/pnas.0903518106

3. A. Bekker, M. E. Barley, M. L. Fiorentini, O. J. Rouxel, D. Rumble, S. W. Beresford, Atmospheric sulfur in Archean komatiite-hosted nickel deposits. *Science* **326**, 1086–1089 (2009). Medline doi:10.1126/science.1177742

4. Q. Guo, H. Strauss, A. J. Kaufman, S. Schroder, J. Gutzmer, B. Wing, M. A. Baker, A. Bekker, Q. Jin, S.-T. Kim, J. Farquhar, Reconstructing Earth's surface oxidation across the Archean-Proterozoic transition. *Geology* **37**, 399–402 (2009). doi:10.1130/G25423A.1

5. J. Farquhar, J. Savarino, S. Airieau, M. H. Thiemens, Observation of wavelength-sensitive mass-independent sulfur isotope effects during SO_2 photolysis: Implications for the early atmosphere. *J. Geophys. Res. Planets* **106**, 32829 (2001). doi:10.1029/2000JE001437

6. A. A. Pavlov, J. F. Kasting, Mass-independent fractionation of sulfur isotopes in Archean sediments: Strong evidence for an anoxic Archean atmosphere. *Astrobiology* **2**, 27–41 (2002). Medline doi:10.1089/153110702753621321

7. Isotopic ratios are usually reported as $\delta^{3x}S$ ($3x$ being either 33, 34, or 36) values where $\delta^{3x}S = 1000 \times [(^{3x}S/^{32}S)_{sample}/(^{3x}S/^{32}S_{VCDT}) - 1] \times 1000$. The terrestrial mass fractionation law is conventionally defined as $\delta'^{33}S = 0.515 \times \delta'^{34}S$, where $\delta'^{3x}S = 1000 \times \ln[(^{3x}S/^{32}S)_{sample}/(^{3x}S/^{32}S_{VCDT})]$ with VCDT the Vienna Canyon Diablo Troilite reference standard. Deviations from this relationship are commonly termed "mass-independent fractionation" and are quantified as $\Delta^{33}S = \delta'^{33}S - 0.515 \times \delta'^{34}S$.

8. I. Halevy, D. T. Johnston, D. P. Schrag, Explaining the structure of the Archean mass-independent sulfur isotope record. *Science* **329**, 204–207 (2010). Medline doi:10.1126/science.1190298

9. J. R. Lyons, Mass-independent fractionation of sulfur isotopes by isotope-selective photodissociation of SO_2. *Geophys. Res. Lett.* **34**, L22811 (2007). doi:10.1029/2007GL031031

10. A. L. Masterson, J. Farquhar, B. A. Wing, Sulfur mass-independent fractionation patterns in the broadband UV photolysis of sulfur dioxide: Pressure and third body effects. *Earth Planet. Sci. Lett.* **306**, 253–260 (2011). doi:10.1016/j.epsl.2011.04.004

11. A. R. Whitehill, S. Ono, Excitation band dependence of sulfur isotope mass-independent fractionation during photochemistry of sulfur dioxide using broadband light sources. *Geochim. Cosmochim. Acta* **94**, 238–253 (2012). doi:10.1016/j.gca.2012.06.014

12. A. R. Whitehill, C. Xie, X. Hu, D. Xie, H. Guo, S. Ono, Vibronic origin of sulfur mass-independent isotope effect in photoexcitation of SO_2 and the implications to the early

earth's atmosphere. *Proc. Natl. Acad. Sci. U.S.A.* **110**, 17697–17702 (2013). Medline doi:10.1073/pnas.1306979110

13. J. P. Grotzinger, J. F. Kasting, New constraints on Precambrian ocean composition. *J. Geol.* **101**, 235–243 (1993). Medline doi:10.1086/648218

14. H. Bao, D. Rumble III, D. R. Lowe, The five stable isotope compositions of Fig Tree barites: Implications on sulfur cycle in ca. 3.2Ga oceans. *Geochim. Cosmochim. Acta* **71**, 4868–4879 (2007). doi:10.1016/j.gca.2007.05.032

15. Y. Ueno, S. Ono, D. Rumble, S. Maruyama, Quadruple sulfur isotope analysis of ca. 3.5Ga Dresser Formation: New evidence for microbial sulfate reduction in the early Archean. *Geochim. Cosmochim. Acta* **72**, 5675–5691 (2008). doi:10.1016/j.gca.2008.08.026

16. D. L. Roerdink, P. R. D. Mason, J. Farquhar, T. Reimer, Multiple sulfur isotopes in Paleoarchean barites identify an important role for microbial sulfate reduction in the early marine environment. *Earth Planet. Sci. Lett.* **331–332**, 177–186 (2012). doi:10.1016/j.epsl.2012.03.020

17. M. J. Van Kranendonk, Volcanic degassing, hydrothermal circulation and the flourishing of early life on Earth: A review of the evidence from c. 3490-3240 Ma rocks of the Pilbara Supergroup, Pilbara Craton, Western Australia. *Earth Sci. Rev.* **74**, 197–240 (2006). doi:10.1016/j.earscirev.2005.09.005

18. L. C. Kah, T. W. Lyons, J. T. Chesley, Geochemistry of a 1.2 Ga carbonate-evaporite succession, northern Baffin and Bylot Islands: Implications for Mesoproterozoic marine evolution. *Precambrian Res.* **111**, 203–234 (2001). doi:10.1016/S0301-9268(01)00161-9

19. S. D. Domagal-Goldman, J. F. Kasting, D. T. Johnston, J. Farquhar, Organic haze, glaciations and multiple sulfur isotopes in the Mid-Archean Era. *Earth Planet. Sci. Lett.* **269**, 29–40 (2008). doi:10.1016/j.epsl.2008.01.040

20. G. Paris, A. L. Sessions, A. V. Subhas, J. F. Adkins, MC-ICP-MS measurement of δ34S and Δ33S in small amounts of dissolved sulfate. *Chem. Geol.* **345**, 50–61 (2013). doi:10.1016/j.chemgeo.2013.02.022

21. Materials and methods are available on *Science* Online.

22. D. Y. Sumner, J. P. Grotzinger, *J. Sediment. Res.* **66**, 419 (1996).

23. G. Hu, D. Rumble, P.-L. Wang, An ultraviolet laser microprobe for the in situ analysis of multisulfur isotopes and its use in measuring Archean sulfur isotope mass-independent anomalies. *Geochim. Cosmochim. Acta* **67**, 3101–3118 (2003). doi:10.1016/S0016-7037(02)00929-8

24. A. J. Kaufman, D. T. Johnston, J. Farquhar, A. L. Masterson, T. W. Lyons, S. Bates, A. D. Anbar, G. L. Arnold, J. Garvin, R. Buick, Late Archean biospheric oxygenation and atmospheric evolution. *Science* **317**, 1900–1903 (2007). Medline doi:10.1126/science.1138700

25. S. Ono, N. J. Beukes, D. Rumble, Origin of two distinct multiple-sulfur isotope compositions of pyrite in the 2.5Ga Klein Naute Formation, Griqualand West Basin, South Africa. *Precambrian Res.* **169**, 48–57 (2009). doi:10.1016/j.precamres.2008.10.012

26. B. S. Kamber, M. J. Whitehouse, Micro-scale sulphur isotope evidence for sulphur cycling in the late Archean shallow ocean. *Geobiology* **5**, 5–17 (2007). doi:10.1111/j.1472-4669.2006.00091.x

27. S. Ono, A. J. Kaufman, J. Farquhar, D. Y. Sumner, N. J. Beukes, Lithofacies control on multiple-sulfur isotope records and Neoarchean sulfur cycles. *Precambrian Res.* **169**, 58–67 (2009). doi:10.1016/j.precamres.2008.10.013

28. D. Papineau, S. J. Mojzsis, Mass-independent fractionation of sulfur isotopes in sulfides from the pre-3770 Ma Isua Supracrustal Belt, West Greenland. *Geobiology* **4**, 227–238 (2006). doi:10.1111/j.1472-4669.2006.00083.x

29. J. Farquhar, J. Cliff, A. L. Zerkle, A. Kamyshny, S. W. Poulton, M. Claire, D. Adams, B. Harms, Pathways for Neoarchean pyrite formation constrained by mass-independent sulfur isotopes. *Proc. Natl. Acad. Sci. U.S.A.* **110**, 17638–17643 (2013). Medline doi:10.1073/pnas.1218851110

30. A. L. Zerkle, M. W. Claire, S. D. Domagal-Goldman, J. Farquhar, S. W. Poulton, A bistable organic-rich atmosphere on the Neoarchaean Earth. *Nat. Geosci.* **5**, 359–363 (2012). doi:10.1038/ngeo1425

31. W. W. Fischer, S. Schroeder, J. P. Lacassie, N. J. Beukes, T. Goldberg, H. Strauss, U. E. Horstmann, D. P. Schrag, A. H. Knoll, Isotopic constraints on the Late Archean carbon cycle from the Transvaal Supergroup along the western margin of the Kaapvaal Craton, South Africa. *Precambrian Res.* **169**, 15–27 (2009). doi:10.1016/j.precamres.2008.10.010

32. N. J. Beukes, Facies relations, depositional environments and diagenesis in a major early Proterozoic stromatolitic carbonate platform to basinal sequence, Campbellrand Subgroup, Transvaal Supergroup, Southern Africa. *Sediment. Geol.* **54**, 1–46 (1987). doi:10.1016/0037-0738(87)90002-9

33. W. W. Fischer, D. A. Fike, J. E. Johnson, T. D. Raub, Y. Guan, J. L. Kirschvink, J. M. Eiler, SQUID-SIMS is a useful approach to uncover primary signals in the Archean sulfur cycle. *Proc. Natl. Acad. Sci. U.S.A.* **111**, 5468–5473 (2014). Medline doi:10.1073/pnas.1322577111

34. M. Baroni, M. H. Thiemens, R. J. Delmas, J. Savarino, Mass-independent sulfur isotopic compositions in stratospheric volcanic eruptions. *Science* **315**, 84–87 (2007). Medline doi:10.1126/science.1131754

35. I. Halevy, Production, preservation, and biological processing of mass-independent sulfur isotope fractionation in the Archean surface environment. *Proc. Natl. Acad. Sci. U.S.A.* **110**, 11244–11249 (2013). Medline doi:10.1073/pnas.1213148110

36. T. Miyano, N. J. Beukes, *S. Afr. J. Geol.* **87**, 111 (1984).

37. B. C. Gill, T. W. Lyons, S. A. Young, L. R. Kump, A. H. Knoll, M. R. Saltzman, Geochemical evidence for widespread euxinia in the later Cambrian ocean. *Nature* **469**, 80–83 (2011). Medline doi:10.1038/nature09700

38. D. Y. Sumner, J. P. Grotzinger, Implications for Neoarchaean ocean chemistry from primary carbonate mineralogy of the Campbellrand-Malmani Platform, South Africa. *Sedimentology* **51**, 1273–1299 (2004). doi:10.1111/j.1365-3091.2004.00670.x

39. A. H. Knoll, N. J. Beukes, Introduction: Initial investigations of a Neoarchean shelf margin-basin transition (Transvaal Supergroup, South Africa). *Precambrian Res.* **169**, 1–14 (2009). doi:10.1016/j.precamres.2008.10.009

40. S. Schröder, J. P. Lacassie, N. J. Beukes, Stratigraphic and geochemical framework of the Agouron drill cores, Transvaal Supergroup (Neoarchean-Paleoproterozoic, South Africa). *S. Afr. J. Geol.* **109**, 23–54 (2006). doi:10.2113/gssajg.109.1-2.23

41. D. Y. Sumner, Late Archean Calcite-Microbe Interactions: Two Morphologically Distinct Microbial Communities That Affected Calcite Nucleation Differently. *Palaios* **12**, 302 (1997). doi:10.2307/3515333

42. D. Y. Sumner, J. P. Grotzinger, Were kinetics of Archean calcium carbonate precipitation related to oxygen concentration? *Geology* **24**, 119–122 (1996). Medline doi:10.1130/0091-7613(1996)024<0119:WKOACC>2.3.CO;2

43. D. Y. Sumner, N. J. Beukes, Sequence Stratigraphic Development of the Neoarchean Transvaal carbonate platform, Kaapvaal Craton, South Africa. *S. Afr. J. Geol.* **109**, 11–22 (2006). doi:10.2113/gssajg.109.1-2.11

44. D. Y. Sumner, thesis (Massachusetts Institute of Technology, 1995); http://hdl.handle.net/1721.1/57758.

45. K. C. Lohmann, J. C. G. Walker, The δ^{18} O record of phanerozoic abiotic marine calcite cements. *Geophys. Res. Lett.* **16**, 319–322 (1989). doi:10.1029/GL016i004p00319

46. D. Y. Sumner, Neoarchean carbonates – Clues to early life and early ocean chemistry. International Association of Sedimentologists, 16th International Sedimentological Congress, 8 to 12 July 2002; http://mygeologypage.ucdavis.edu/sumner/IAS/IAS_A6.pdf.

47. J. F. Truswell, K. A. Eriksson, Stromatolitic associations and their palaeo-environmental significance: A re-appraisal of a lower proterozoic locality from the northern cape province, South Africa. *Sediment. Geol.* **10**, 1–23 (1973). doi:10.1016/0037-0738(73)90008-0

48. D. Y. Sumner, S. A. Bowring, U-Pb geochronologic constraints on deposition of the Campbellrand Subgroup, Transvaal Supergroup, South Africa. *Precambrian Res.* **79**, 25–35 (1996). doi:10.1016/0301-9268(95)00086-0

49. S. Bohic, K. Murphy, W. Paulus, P. Cloetens, M. Salomé, J. Susini, K. Double, Intracellular chemical imaging of the developmental phases of human neuromelanin using synchrotron X-ray microspectroscopy. *Anal. Chem.* **80**, 9557–9566 (2008). Medline doi:10.1021/ac801817k

50. A. Das, C.-H. Chung, C.-F. You, M.-L. Shen, Application of an improved ion exchange technique for the measurement of δ^{34}S values from microgram quantities of sulfur by MC-ICPMS. *J. Anal. At. Spectrom.* **27**, 2088 (2012). doi:10.1039/c2ja30189j

51. T. Ding, S. Valkiers, H. Kipphardt, P. De Bièvre, P. D. P. Taylor, R. Gonfiantini, R. Krouse, Calibrated sulfur isotope abundance ratios of three IAEA sulfur isotope reference materials and V-CDT with a reassessment of the atomic weight of sulfur. *Geochim. Cosmochim. Acta* **65**, 2433–2437 (2001). doi:10.1016/S0016-7037(01)00611-1

52. S. Ono, B. Wing, D. Johnston, J. Farquhar, D. Rumble, Mass-dependent fractionation of quadruple stable sulfur isotope system as a new tracer of sulfur biogeochemical cycles. *Geochim. Cosmochim. Acta* **70**, 2238–2252 (2006). doi:10.1016/j.gca.2006.01.022

53. J. E. Johnson, S. M. Webb, K. Thomas, S. Ono, J. L. Kirschvink, W. W. Fischer, Manganese-oxidizing photosynthesis before the rise of cyanobacteria. *Proc. Natl. Acad. Sci. U.S.A.* **110**, 11238–11243 (2013). Medline doi:10.1073/pnas.1305530110

54. J. E. Johnson, A. Gerpheide, M. P. Lamb, W. W. Fischer, O2 constraints from Paleoproterozoic detrital pyrite and uraninite. *Geol. Soc. Am. Bull.* **126**, 813–830 (2014). doi:10.1130/B30949.1